PAPER • **OPEN ACCESS**

Effect of varying ethanol and water compositions on the acetone sensing properties of WO_3 for application in diabetes mellitus monitoring

To cite this article: Valentine Saasa *et al* 2020 *Mater. Res. Express* **7** 035905

Materials Research Express

PAPER

Effect of varying ethanol and water compositions on the acetone sensing properties of WO_3 for application in diabetes mellitus monitoring

Valentine Saasa[1,2], **Yolandy Lemmer**[3], **Thomas Malwela**[1], **Amos Akande**[5,6], **Mervyn Beukes**[4] and **Bonex Mwakikunga**[1,7]

[1] DSI/CSIR-Centre for Nanostructures and Advanced Materials, PO Box 3951, South Africa
[2] Department of Biochemistry, Genetics and Microbiology, University of Pretoria, Pretoria 0001, South Africa
[3] CSIR-Next Generation Health, Pretoria, 0001, South Africa
[4] Department of Biochemistry, Stellenbosch University, Western Cape, South Africa
[5] University of Limpopo, Department of Physics, P/Bag X1106, Sovenga, 0727, South Africa
[6] CSIR NextGen Enterprises and Institutions, Advanced Internet of Things, P O Box 395, Pretoria, 0001, South Africa
[7] Department of Physics, Tshwane University of Technology, PO Box 680, Pretoria 0001, South Africa

E-mail: bmwakikunga@csir.co.za

Keywords: acetone, gas sensor, tungsten trioxide, selectivity, sensitivity

Supplementary material for this article is available online

OPEN ACCESS

RECEIVED
10 January 2020

REVISED
10 February 2020

ACCEPTED FOR PUBLICATION
6 March 2020

PUBLISHED
23 March 2020

Abstract

Tungsten oxide based gas sensors have attracted a lot of attention in breath acetone analysis due to their potential in clinical diagnosis of diabetes. The major problem with this material in sensor application has been remarkable response to all gases but low selectivity to specific gases. Herein, we report the gas sensing performance of WO_3 materials which were synthesized by varying water and ethanol ratios using a facile solvothermal method for acetone detection. The gas sensing properties of as-prepared WO_3 were tested on acetone C_7H_8, NO_2, NH_3, H_2S and CH_4 under relative humidity. X-ray diffraction patterns show that as-prepared WO_3 samples are mainly composed of monoclinic WO_3, a phase having relatively high selectivity to acetone. The as-prepared WO_3 sensors produced using 51:49 ratio of water: ethanol show an increase in acetone response as the acetone concentration increases and a decrease in acetone response as the relative humidity increases. The sensor responded to a very low acetone concentration ranging from 0.5 to 4.5 ppm which is normally found in human breath. Furthermore, the sensor exhibited high sensitivity and selectivity to low ppm of acetone at 100 °C. On contrary, the sensor showed significantly lower response to other gases tested.

1. Introduction

Tungsten trioxide (WO_3), an n-type semiconductor with a band gap ranging from 2.4 and 2.8 eV, chemically stable and with a reasonably high electrical conductivity; has attracted a lot of interest in gas sensing [1–5]. Lately, more research has focused on its remarkable gas sensitivity which makes it an ideal candidate for different gases i.e., acetone, H_2S, sulphur dioxide (SO_2), CO, ethanol, hydrogen (H_2) and NH_3 [6–8]. According to literature, WO_3 has been reported to exhibit various crystal phases, which includes monoclinic I (γ-WO_3), monoclinic II (ε-WO_3), and orthorhombic (β-WO_3). Among the above, mentioned phases, γ-WO_3 is considered a promising phase for detection of acetone, while ε-WO_3 has high selectivity to acetone [9–11]. Although ε-WO_3 has been reported to have high selectivity [12–14], is also said not to be stable at high temperature [15], and it is usually becomes stable after doping with Cr or incorporating Si into the lattice of WO_3 [16].

To achieve desired phases, different efficient methods and techniques such as sol-gel route [17], electrospinning [18], hydrothermal methods [10], chemical vapour deposition [19], physical vapour deposition [20], etc were used. For example, Righettoni *et al* [13] have reported Si-WO_3 nanoparticles synthesises by flame spray pyrolysis. This study reported that annealing play a major role in the formation of various tungsten crystal

phases. Furthermore, it is well known that morphology of nanostructured have a great effect on the properties, particularly sensing effect [21]. The control of morphology study has attracted a lot of interest due to desirable properties such as high aspect ratio structure, large surface area, good sensing and optical properties. Additionally, controlling morphology and crystal structure works very well for tungsten oxides as it has various crystal phases which might play a crucial role in achieving desired sensing properties.

With so much great work done in controlling the morphology and crystal structures of materials, there are few works reported on the effect of solvothermal on a low ppm concentration of acetone and low operating temperature. Chen *et al* [3] reported a solvothermal synthesis of tungsten oxides with various morphologies and their acetone sensing properties at 300 °C. They have found a good response at 100 ppm. Epira *et al* [22] reported the good acetone performance of TiO_2 modified with tungsten species at a working temperature of 200 °C. The low acetone (20 ppm) performance of copper-doped tungsten sensor was reported [18]. Besides the sensor not being pure WO_3, the operating temperature was 300 °C. Huang *et al* [23] found a sensitive acetone flower-like sensor at working temperature of 320 °C, after annealing the sample at 400 °C. All the mentioned great works are however not good enough for potential use in diabetic diagnosis as they report high acetone concentration and at high working temperature.

WO_3 is among the transition metal oxides having interesting properties such as high surface areas, portability, low-cost and easiness of use which are promising candidates in the field of breath analysis [24]. In nanomedicine, early diagnosis and monitoring of the diseases is considered a need in the world; especially for diabetes mellitus due to continuous painful pricking [25]. The exhaled human breath has been widely used as a potential alternative for the study and diagnosis of medical conditions [26, 27]. Furthermore, it contains hundreds of VOCs ranging from part-per-trillion (ppt) to part-per-million (ppm) in concentration [28, 29]. These include isoprene, methanol, acetone, and several inorganic gas molecules such as nitrogen oxide (NO), carbon monoxide (CO) and hydrogen sulphide (H_2S). Breath acetone has been found to correlate well with blood glucose from diabetic patients [30]. Hence the optimization of WO_3 phase composition and sensing performance are crucial for stable and reliable detection of acetone.

Herein we report, without the expensive high-temperature annealing, the facile synthesis of different tungsten crystal phases and morphologies, using solvothermal method. This method allows for change in crystalline phase, which includes monoclinic $W_{18}O_{49}$, hexagonal WO_3, and monoclinic WO_3, by varying the solvent composition. Different solvents and water contents were varied in order to change the crystal phase of WO_3 from hexagonal to monoclinic. The sensing properties of as-prepared tungsten oxides were examined by measuring the sensor response of main VOCs such as acetone, toluene, and other gases such as hydrogen sulphide (H_2S), ammonia (NH_3), Nitrogen dioxide (NO_2) and methane (CH_4). The nanorod synthesised with 49:51 ethanol: water sensor exhibited a high response, and good selectivity to low ppm of acetone at relatively lower operating temperature (100°C). The results indicate that the WO_3 based sensors can be very beneficial in designing sensors for detection of acetone in point of care diagnosis.

2. Materials and methods

2.1. Materials

Tungsten hexachloride (wcl_6) and 90% ethanol were purchased from Sigma Aldrich and were used without further treatment.

2.2. Synthesis of nanostructured tungsten oxides

This work reports a facile method for synthesis of tungsten oxide nanostructures with varying morphologies such as nanorods, nanocubes, and nanorods mixed nanoparticles as shown in the schematic diagram in figure 1. The process also enables for the change in crystalline phase, such as monoclinic $W_{18}O_{49}$, hexagonal WO_3, and monoclinic WO_3, by varying the composition of the solvent. An amount of 4.05 g of tungsten hexachloride was dissolved in 100 ml of ethanol as a stock solution. To prepare the tungsten trioxides nanostructures, an amount of 10 ml of the stock solution was mixed with the following ratios of ethanol and water. Sample 1, named S1 was based on as-purchased ethanol (90% ethanol: 10% water), sample 2 (S2) was 1:9 of water: 90% ethanol translating to ~18 water content, sample 3 (S3) was 51:49 of water: ethanol and sample 4 (S4) was based on pure D.I water translating to 92% water content. The solution was then transferred to a 100 mL Teflon-lined acid digestion bombs. The reaction was run at 200 °C for 10 h using an electric oven. After, the as-prepared were collected and washed by centrifugation to remove any impurities.

2.3. Fabrication of sensors and sensing measurements

The sensor device was prepared using the alumina interdigitated electrodes (2 mm x 2 mm) with one sided having pt-electrode and one side having micro-heater that is used for gas sensing measurements. The as-prepared

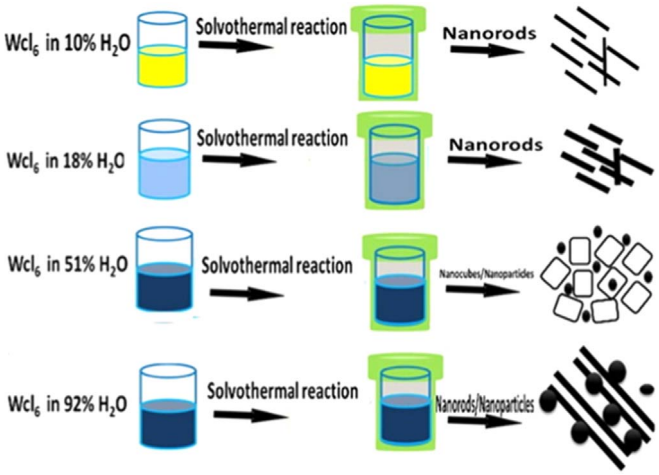

Figure 1. Schematic diagram showing the solvothermal synthesis of $W0_3$ nanostructures.

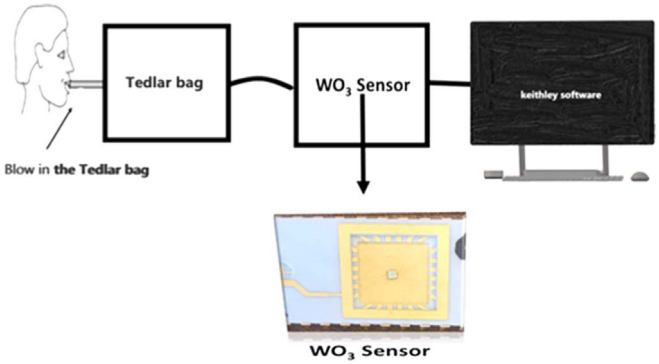

Figure 2. Schematic diagram of breath analysis from a volunteer using tedlar bag for sampling and $W0_3$ sensor device.

nanostructured powders were dissolved in ethanol to form a paste and drop casted the paste uniformly onto the pt-electrodes of alumina substrate. The impregnated substrate was then heated at 100 °C for 1 h to remove the solvent and for adhesion of the paste. The gas sensing measurement was conducted using a gas sensing station KSGAS6S (KENOSISTEC, Italy). The measurements were tested at 50 °C, 75 °C, 100 °C, 150 °C and 200 °C by changing the voltage. Synthetic air with a constant flow rate of 0.5 l min^{-1} was used as a carrier gas. The acetone gas was tested at a varying humidity ranging from 0, 10, 20, 40, 60, 80%RH to best suit application in breath acetone detection. Other gases tested includes toluene, nitrogen dioxide, ammonia, hydrogen sulphide and methane. The sensor response was defined as Ra/Rg where Ra is the resistance of the sensor in dry air and Rg is the resistance of the sensor in the target gas.

2.4. Exhaled breath analysis

The Exhaled breath measurements were conducted with the tedlar bag connected to a box which houses WO_3 sensor as shown in figure 2. The sensor was connected to the 2 electrode probes (keithley, semiconductor characterization system) for resistivity measurements. Acetone gas was first tested on the sensor to identify the correct voltage for acetone and it was found to be −10 v. Followed by running the acetone gas standards ranging from 0.5, 1.0, 15, 2.0 ppm and diabetic and non-diabetic breath at set voltage of −10 V.

3. Results and discussion

3.1. X-ray diffraction

The effect of varying solvent mixing ratios during the synthesis of WO_3 samples was examined by x-ray diffraction (XRD). Figure 3 depicts the XRD patterns of the as-prepared tungsten oxides, which show that phase composition and intensities of the reflections from different planes depended on solvent mixing ratio. The diffraction peaks of sample (S1) prepared with ethanol only could be indexed to the standard hexagonal WO_3

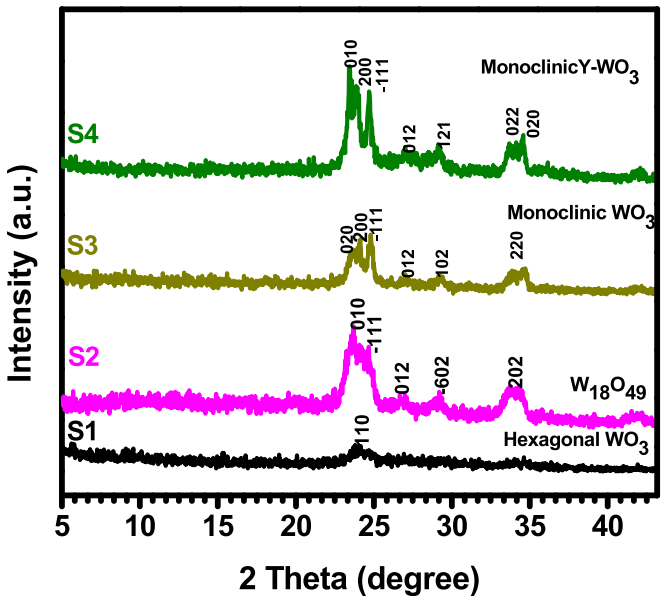

Figure 3. The XRD patterns of the as-prepared WO_3 nanostructures obtained after varying solvent content from pure ethanol. The diffraction peaks of sample (S1) prepared with ethanol only compared with the standard hexagonal WO_3 (JCPD: 33–1387), the S2 prepared with 9:1 EOH: H_2O compared with standard W18O49, (JCPDS: 05–0392) and S3 (1:1 EOH: H_2O) and S4 (H_2O-only) with increased water content compared to monoclinic WO_3 (JCDPS: 00–0043–1035).

(JCPDS: 33–1387), and the one (S2) prepared with 82:18 EOH: H_2O could be indexed to the standard W18O49, (JCPDS: 05–0392). When the water content was increased in the remaining two samples (S3 and S4), the monoclinic WO_3 (JCDPS: 00–0043–1035) was observed. The results observed in here are in agreement with the HRTEM study which is discussed later in the paper. Using the Bragg's equation $n\lambda = 2d \sin\theta$, where d is the inter-planar-spacing observed on HRTEM images, we found that the 2θ correlate well on all the samples.

The predominance of (010) plane shows that the WO_3 nanorods grew along the [010] direction. Furthermore, it can be seen that the (010) plane is parallel with the (020) which corresponds with the layered rods on the scanning electron microscopy micrograph. When the water content increases, we observed the monoclinic WO_3 (JCDPS: 00–0043–1035) in both samples with 51:49 and 18:82 (ethanol: water) ratios (see figure 4). The results confirm that the amount of water in the solvent can control the crystallinity of tungsten oxide. It was worth noting that the oxygen which was in water contributed to the formation of tungsten oxides crystalline phases. Furthermore, the crystallite size D of the dominating peak (010) was calculated using Scherer's equation:

$$D = \frac{0.9\lambda}{\beta \cos\theta} \tag{1}$$

Where λ and β are the wavelength of CuKα radiation and the FWHM of the (010) peak. It was noted that the crystallite size D of the material decreases with an increase in water (see table 1). Since Trinh *et al* [31] highlighted that the metal oxides sensor's response is mainly dependent on the crystallite size of the material of interest being tested. This indicates that as the grain size decreases, there will be an improvement of the gas sensor response to gases. When the grain size is comparable to 2 L (L being the thickness of the layer), D = 2 L a space charge develop in the region of crystallite and maximum response will be achieved.

3.2. Morphological characterization

The effect of varying solvent mixing ratios on the morphology and microstructure of WO_3 were further examined using SEM and HRTEM, respectively. The wet chemical synthesis enables the control of the particle size, shape, and the possibility of large-scale production as compared to the physical synthesis. Tungsten oxide nanostructures having different morphologies of one-dimensional nanostructures, such as nanorods, nanocubes mixed with nanoparticles and nanorods mixed with nanoparticles, were produced by solvothermal process. Figure 4 shows the SEM morphologies of WO_3 obtained from samples synthesized by varying the solvent contents. As can be seen from figure 4 that as the content of water in solvent is increased, the shape of the particles changed from rod-like structures in figure 4(a), nanorod-like structures in figure 4(b), a mixture of nanoparticles and cube-like structures in figure 4(c) to a mixture of larger nanorods and nanoparticles in figure 4(d). Thus, samples prepared using high ethanol content produced nanorod-like structures while the ones prepared using high water content cube-like structures, nanorods mixed nanoparticles. As seen from XRD

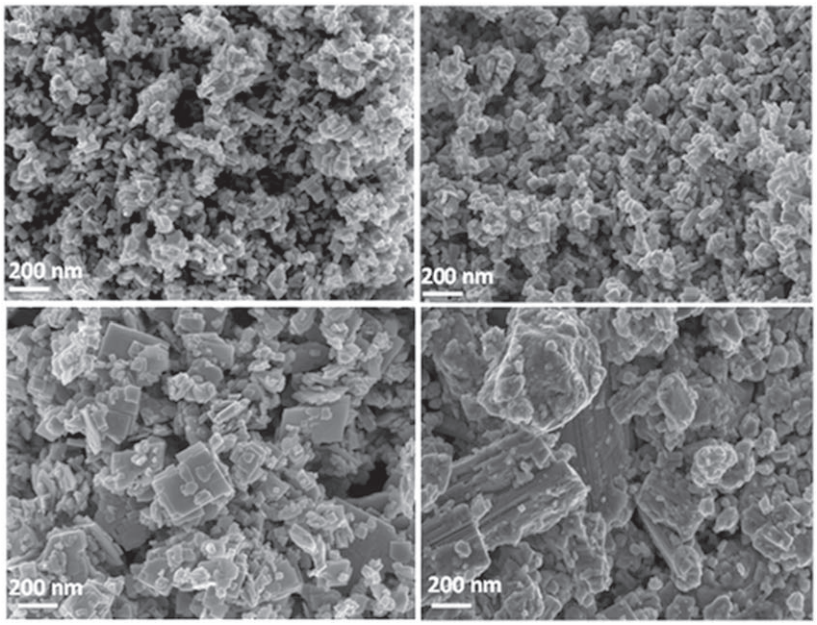

Figure 4. SEM morphologies of the as-prepared WO_3 nanostructures obtained after varying solvent from (a) pure ethanol to (b) 1:9 (ethanol: water), (c) 1:1 (ethanol: water) and (d) pure water.

Table 1. Summary of the surface area, crystallite size and dielectric constants.

Sensor	p_{water}	Surface area	Pore diameter	Crystallite size
S1	10	73.16	4.47	11.36
S2	18	12.35	3.61	8.02
S3	51	14.77	11.63	7.51
S4	92	70.35	4.05	7.74

results, SEM observations also confirm that the morphology of WO_3 was controlled by varying the compositions of water and ethanol during solvothermal process.

HRTEM morphologies in figures 5(a)–(d) is in good agreement with SEM in figures 5(a)–(d) that when the solvent composition changes, the morphology also changes. Interestingly, the HRTEM micrograph in figure 5(b), indicates that the nanorod grew along the [010] direction, which is also in agreement with the XRD. Moreover, these results show that the composition of the solvents plays a major role in the formation of morphology and crystalline phase of tungsten oxide, like nanorods $W_{18}O_{49}$, hexagonal rods-like WO_3, and nanorods WO_3 [32, 33]. HRTEM study also confirmed the crystallite size and different phases as observed with XRD. Using the Bragg's equation, phases were confirmed and the XRD results are found to be in agreement with the HRTEM. The crystallite size of S1, S2, S3, S4 were found to be ~11.3, 8.0, 7.5 and 7.7, respectively. The crystallite estimation is in accordance with the size calculated using Scherer's equation. As the ratio of water and ethanol is nearly equal, crystallite size decreases and increases when there is nearly pure ethanol and water as a solvent. This trend is also observed on the surface area and XRD analysis. Therefore, the sample produced with nearly equal ratio of water to ethanol is expected to have the highest response to acetone gas as compared to other samples. The gas sensing will be discussed in detail later.

3.3. Proposed growth mechanism-the Wang *et al* model

From the SEM and HRTEM observations, we have learned that the water in the reaction controls the phase and morphologies of the as-prepared tungsten oxide nanostructures. This is consistent with the mechanism proposed by Wang *et al* [34] wherein the formation of WO_3 takes place, firstly by nucleation and secondly by subsequent growth. For nucleation, the samples prepared in the non-aqueous system, ethanol slowly decompose as illustrated in reaction (1) with simultaneous release of water molecules, which coordinates the W^{6+} cations to form tungsten oxy/hydroxychloride complexes ($[W(OH)xCln]^{6-(n+x)}$ or $[WOyCln]^{6-(n+2y)}$). Afterwards, WO_3 nuclei are produced along with the condensation/polymerization of the complexes (reaction (2)).

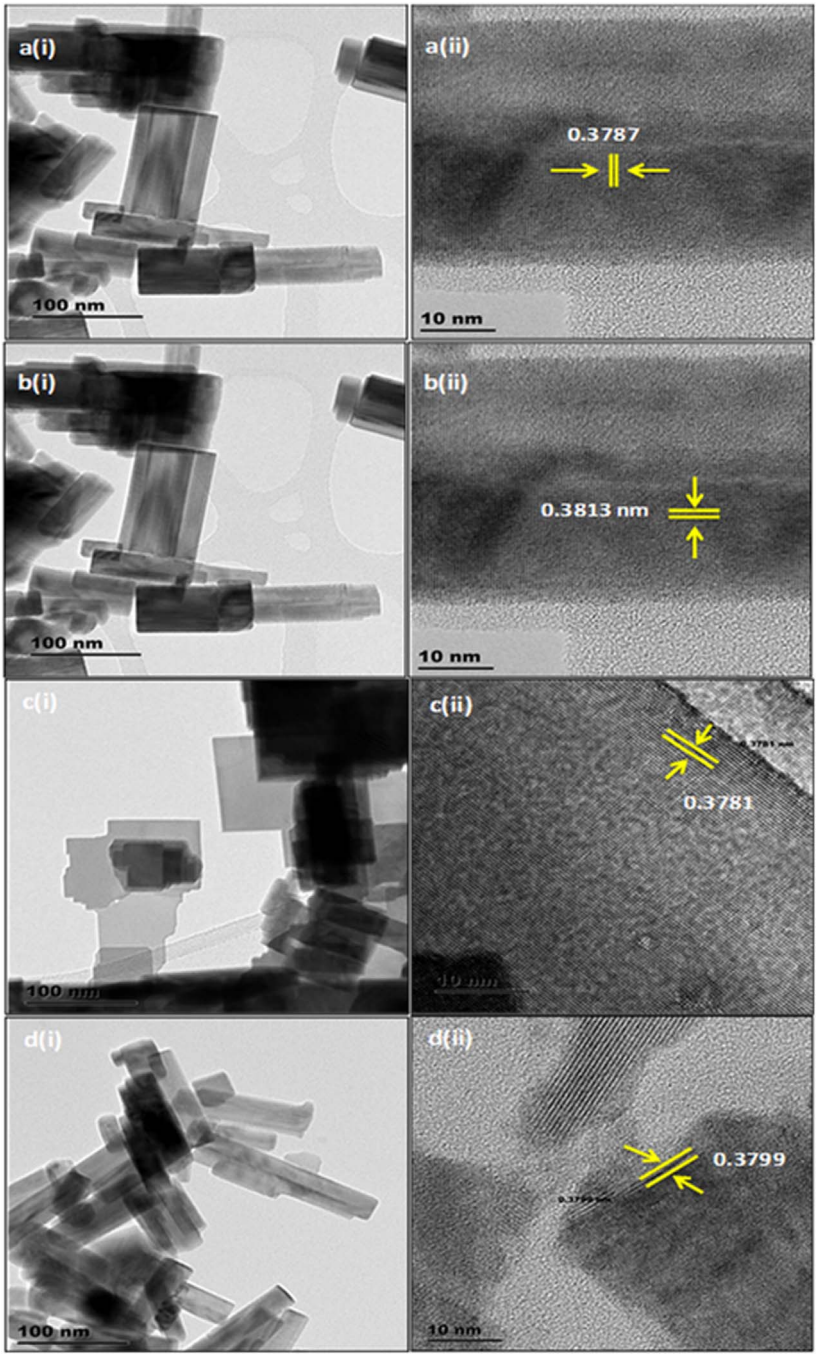

Figure 5. HRTEM morphologies of the as-prepared WO_3 nanostructures obtained after varying solvent from (a) pure ethanol to (b) 1:1 (ethanol: water), (c) 1:9 (ethanol: water) and (d) pure water.

$$\mathbf{CH_3CH_2OH \rightarrow CH_2CH_2 + H_2O} \quad (2)$$

$$\mathbf{WCl_6 + 3H_2O \rightarrow [W(OH)_xCl_n]^{6-(n+x)}}$$

Or

$$\mathbf{[W(O)_yCl_n]^{6-(n+y)}\, WO_3 + 6HCl} \quad (3)$$

3.4. Proposed growth mechanism-current model

The Wang *et al* model is good for the reaction of WCl_6 with H_2O in the absence of ethanol. Also the reaction of WCl_6 directly with H_2O is energetically expensive. For instance, it requires a lot more energy (ΔH°_f (298 K) $= -1693$ kJ mol^{-1}) to dissociate water into H^+ and OH^- than dissociate ethanol (ΔH°_f(298 K) -178 kJ mol^{-1}) into $CH_3CH_2O^- + H^+$. In accordance with the Kirchhoff's law applied to chemical reactions, one would expect WCl_6 to react more with ethanol than with water. Based on simple current-divider model

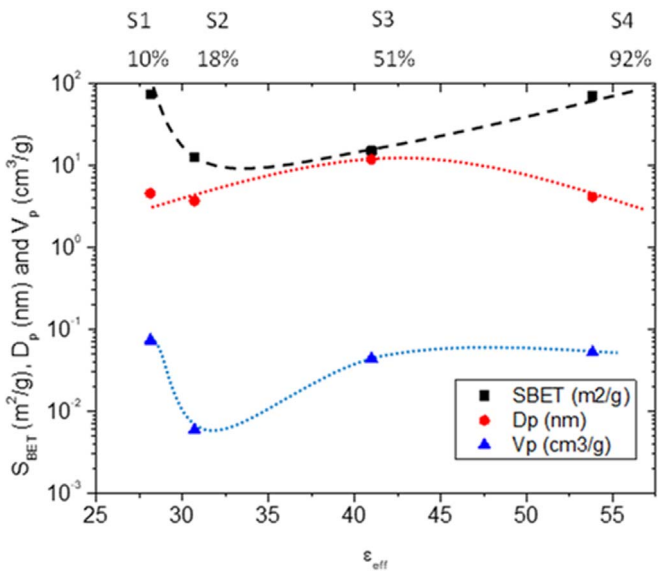

Figure 6. Surface properties of S1, S2, S3, and S4 against the corresponding dielectric constants of the ethanol-water solvents and the water content in the mixture.

where chemical potential powering a reaction has two pathways running in parallel with enthalpies (or activation energies) of such pathways represented as resistances, it can be shown that one can calculate the relative probabilities of WCl_6 reacting with ethanol or water to be 88% or 12% respectively.

This calculation shows that although ethanol is more likely to take charge in the reactions, the WCl_6 reaction cannot be entirely trivialized as there is still 12% chance. This analysis explains why the final WO_3 produces from the ethanol-water solvent will have phases, composition (stoichiometry) and morphology dependent on the composition of ethanol and water in the said solvent.

3.5. Predicting the properties of ethanol-water mixture/solvent and its effects on the final WO_3 morphology

We refer to a classic theory called effective medium theory [35] for us to calculate the properties of the ethanol-water mixture of various compositions of ethanol and water which is presented by equation (3). The dielectric constants are presented in figure 7 against the BET surface and water-ethanol ratios. More details on the effect of solvent ratio on the sensing properties is discussed on section 3.7. For instance we can estimate the water-composition dependency of the dielectric constant of the ethanol-water mixture as follows;

$$\varepsilon_{eff} = \varepsilon_{ethanol} + 3p_{water}\varepsilon_{ethanol}\frac{\varepsilon_{water} - \varepsilon_{ethanol}}{\varepsilon_{water} + 2\varepsilon_{ethanol}} \quad (4)$$

The dielectric constant of water is $\varepsilon_{water} \sim 79$ and that of ethanol $\varepsilon_{ethanol} \sim 25$. Given the composition of water, p_{water}, it is then possible to estimate the effective dielectric constant of the mixture. This can be used to predict other properties of the ethanol-water such as density, reactivity and the like. The effective dielectric constants calculated from this equation are tabulated in table 1 and figure 6, as an illustration and these are correlated with other properties of the finally WO_3 materials as will be discussed in later sections.

3.6. Brunauer–Emmett–Teller (BET) analysis

The dielectric The BET analyses were conducted to give more insight on the porous nature of WO_3 structures and effect of varying solvent mixing ratios. The characteristics such as the surface area, volume and pore size of WO_3 nanostructures are summarized in table 1 and S1 (supplementary is available online at stacks.iop.org/MRX/7/035905/mmedia). It has been observed that the surface area increased for sample S1 prepared by nearly pure ethanol and decreased for samples S2 and S3 prepared by 51:49 of ethanol: water ratios, and later increased for sample S4 where nearly only water was used as a solvent. This observation is consistent with the crystallite size observed with XRD and HRTEM. The pore volume decreased with the addition of water, however high pore diameter of about 10.54 nm was observed at a solvent ratio of 51:49 (ethanol: water) as compared to other samples, i.e., sample S3 having the largest value of D_P (pore diameter). It may not have the largest S_{BET} (surface area per unit mass) and it may also not have the largest V_P (the volume of the pore per unit mass) but the fact that it has the largest D_p suggests that D_p gives it the biggest advantage to sense acetone over the other samples.

Furthermore, the porous structure of the as-synthesised tungsten oxides indicates that there was removal of the solvents and interspaces among the assembled nanorods and particles. These WO_3 nanostructures with

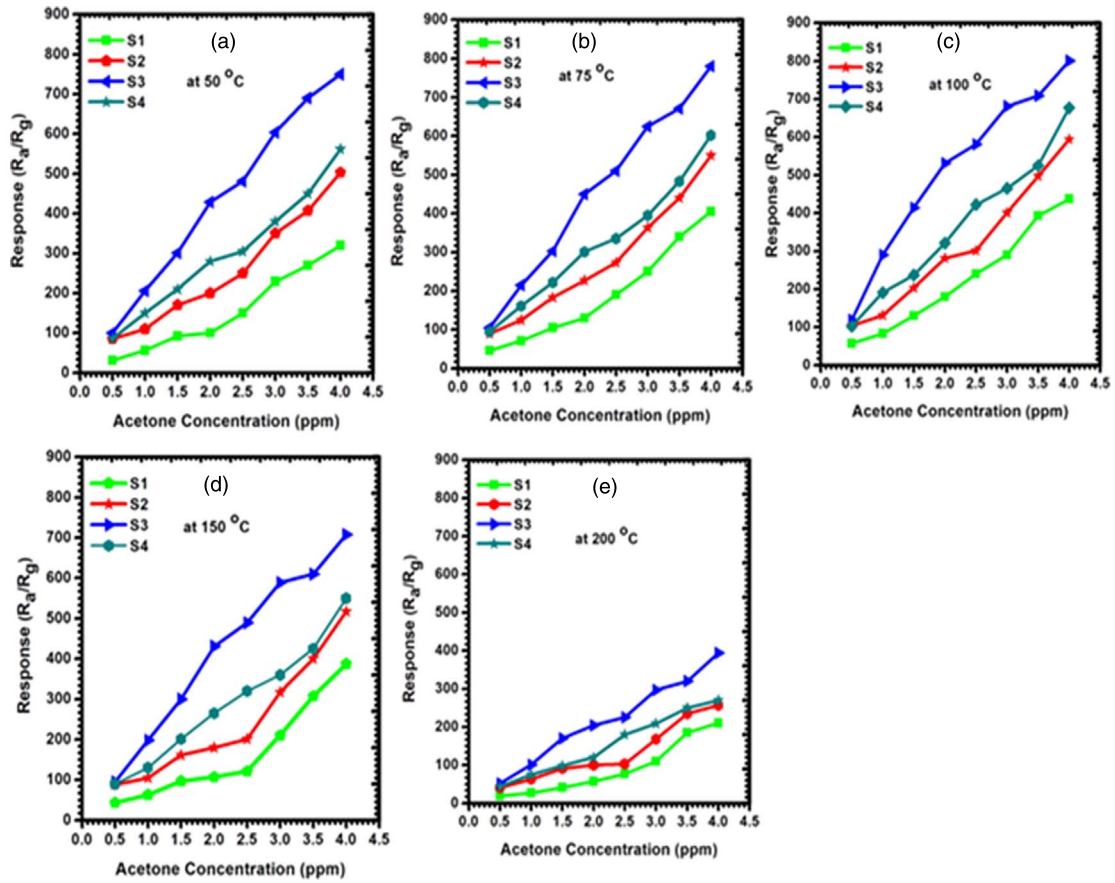

Figure 7. Response versus acetone concentration for samples synthesised with varying solvent composition at (a) 50 °C, (b) 75 °C (c) 100 °C, (d) 150 °C and (e) 200 °C.

higher surface areas and porosity play a significant role in the performance of sensing materials. Our results agree very well with the sensing results which will be discussed later. The sample with higher pore diameter showed a higher response and selectivity to acetone as compared to the sample with higher surface area. As it was also observed and mentioned by Tshabalala *et al* [36], a large surface area alone does not influence the good sensing response, it is however influenced by the porous surface which ultimately allows the gas to be adsorbed into the whole sensing layer, enhancing the response of the sensor.

3.7. Gas sensing properties of WO_3 sensors

The sensing performances of WO_3 samples synthesized by varying solvent mixing ratios to acetone concentration ranging from 0.5 to 4.5 ppm were investigated at 50, 75, 100, 150 and 200 °C, respectively. As we know, the acetone concentration in human can be 0.8 ppm to lower and for diabetic patients' ranges from above 0.8 ppm. Figures 7(a)–(e) shows the dynamic response curves of the sensors. All the sensors demonstrated an increase in sensors response upon an increase in acetone concentration. This behaviour is common for the semiconducting metal oxides including WO_3. It can be described by the kinetics and mechanics of gas adsorption and desorption [37]. Additionally, the n-type semiconductor metal oxides have been proven to have great sensing properties for reducing gases [36].The gas sensing response (R) is defined as:

$$R = \frac{R_a}{R_g} \tag{5}$$

Where Ra and Rg, represent the resistance of the sensor in dry air and the target gas, respectively.

The dielectric Sensor S3 showed the highest response to acetone in all temperatures as compared to other sensors. For example, the response of 2 ppm acetone at 50 °C was 1.9, 2.4, 5.3, and 3.42 for S1, S2, S3 and S4, respectively, the response at 100 °C was 172.82, 278.53, 534.93 and 321.05, respectively. In the two mentioned temperatures, the response of S3 was almost double times higher than all the samples. This was also observed in the two remaining temperatures (150 and 200 °C). This could be attributed to the high pore diameter and monoclinic phase. The high pore diameter in this case plays a crucial role as it offers more sites for surface adsorption and desorption of acetone. Interestingly, the results obtained in here are not entirely surprising that

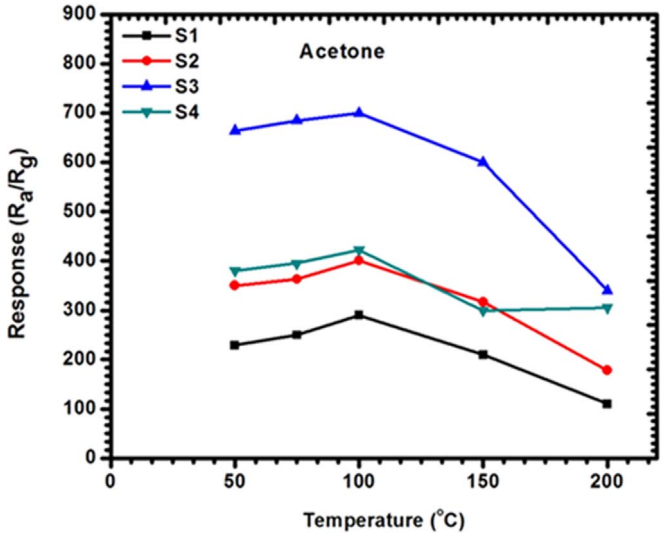

Figure 8. Response of sensor synthesised with varying solvent composition to 2 ppm of acetone at different operating temperatures (50 °C–200 °C).

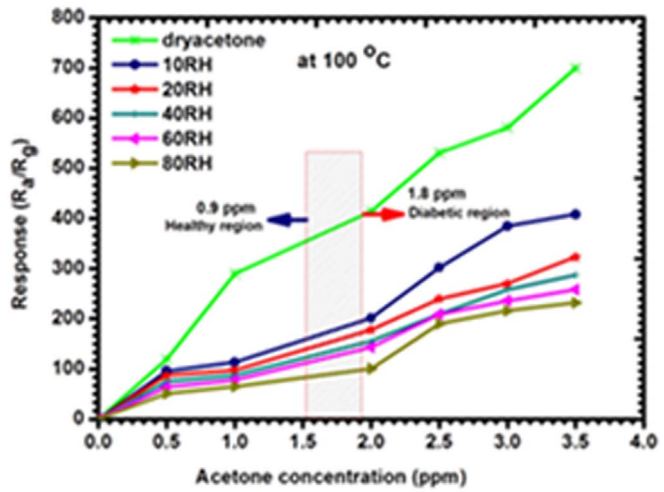

Figure 9. Sensor (S3) responses to acetone concentration (0–4 ppm) at varying RH from 0 to 60% at 100 °C. Diabetic patient (>1.8) can be clearly distinguished from healthy patients (<0.9) by, at least, 67% difference in sensor response.

the high surface area does not always contribute to excellent sensing response. Tomer *et al* [38] and Tshabalala *et al* [36] also observed the same findings. Sample S3 has less surface area as compared to other samples but showed high response in all temperatures.

We observed an increase in sensor response from 50 °C, 75 °C, and 100 °C with the highest respond at 100 °C, and a decrease from 150 °C and 200 °C as shown in figure 8. When the heating temperature is low, the chemical activation of nanoparticles, nanorods and nanoplates can be low and consequently result into a low response. However, increasing the temperature usually leads to a positive chemical activation, with the gas sensor demonstrating maximum response at the operating temperature of 100 °C. This temperature was therefore selected as operating temperature for further investigation in this study. More interestingly, all the sensors could respond to even a low concentration (0.5 ppm). This gives an advantage to the current sensors in an application that requires low concentration detection of acetone especially for diabetes mellitus monitoring and management. As most good performing acetone sensors are achieved at high ppm concentration for example this study [16], the Y-doped SnO_2 showed the good acetone performance at 50 ppm.

Figure 9 depicts that when S3 sensor is exposed to dry acetone, the response increases with increasing acetone concentration. However, the response to acetone decreased with an increasing RH%. This is attributed to the fact that more sensing sites of the sensor were occupied by a gaseous H_2O with the increase of RH%. Therefore, the concentration of chemisorbed oxygen on the sensor will decrease and results in the weakened

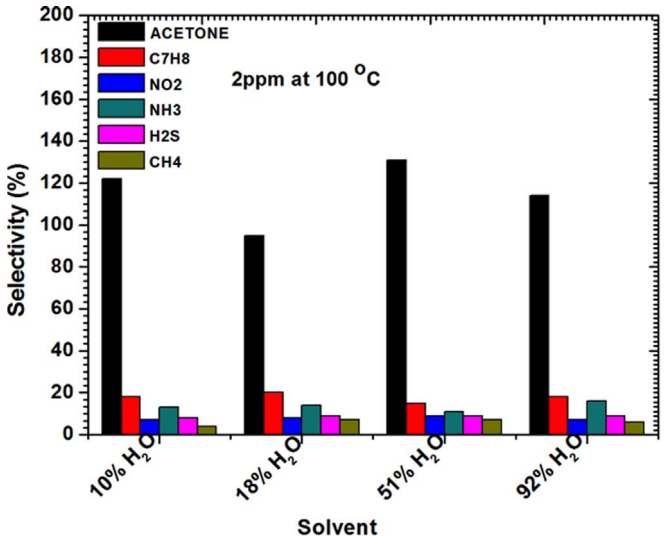

Figure 10. Selectivity values of sensor produces with varying solvent content against varying gases at 100°C at 2 ppm concentration.

acetone response. Furthermore, this plot can also clearly distinguish a diabetic patient region and a healthy patient region. The response to dry acetone is 1.3 and for acetone at 60 RH% (ambient relative humidity in human breath) is 0.64 both tested at 1 ppm. The difference in sensor response is 0.66; this makes it possible for the diagnosis and monitoring of diabetes mellitus by using breath acetone.

In gas sensors, selectivity is one of the key parameter more especially gas sensor for disease detection to ensure correct diagnosis and avoid false positive results. To perform the selectivity test, we used the selectivity (σ) equation [39]:

$$\sigma = \frac{R_{gas}}{R_{gas1} + R_{gas2} + R_{gas3} + R_{gas4} + \ldots + R_{gasN}} \times 100$$

Where R_{gas}, is the gas of interest and $R_{gas1} + R_{gas2} + \ldots + R_{gasN}$, is the sum of all gases.

The values for selectivity of the gases against the sensors were calculated from the responses obtained from 2 ppm at 100 °C are presented in table S2 on the supplementary results. The results show that all the sensors select acetone better than any other gases, however, sample S3 showed the highest selectivity. The high sensitivity and response of S3 could be influenced by high pore diameter, small crystallite size and plate-like morphology. It has been reported that the pore diameter can positively influence the sensitivity of the sensor [40–42].

When the values of the morphological properties in table 1 of the final WO_3 samples are plotted against the corresponding dielectric constants of the ethanol-water solvents and the water content in the mixture thereof, the profiles as shown in figure 6 are obtained. These profiles suggest that both specific surface area and specific pore volume have similar trajectories with a minimum values between sample 2 and sample 3 whereas specific pore diameter has a definite maximum in sample 3 where the solvent had a water content of 51% and an effective dielectric constant of 42.

We further used selectivity data on table S2 (on supplementary materials) and plotted against all the gases at 2 ppm and 100 °C. As can be seen from figure 10, we observed that acetone shows magnificent selectivity towards acetone in all the sensors as compared to other gases. An ideal sensor should have selectivity of 100% to one gas and 0% to all; however there is a huge gap between an acetone gas and other tested gases. The high selectivity and response of sample S3 could be attributed to small crystallite size, porous morphology and stabilization of ε-WO_3 monoclinic phase which has strong interaction force between electric dipole of ε-WO_3 and the largest dipole moment of acetone [13, 43]. Furthermore the ε-WO_3 phase is best in detecting [7] and selecting acetone. The highest response, excellent selectivity, ability to respond well at varying humidity of the sample S3 which is produced by a very simple and cheap method shows a possibility of future application in breath acetone detection for diabetes mellitus monitoring.

We have gathered the gas sensing performances of materials reported in literature and compared it with this present work, the summary is shown in table 2. Among these materials, it can be seen that WO_3 (S3 sensor) showed a good response at low operating temperature, without doping or functionalization. Furthermore, this also opens more research scope on non-invasive way of monitoring diabetes mellitus using the breath acetone. This makes it a promising material towards the development of sensors for the detection of acetone.

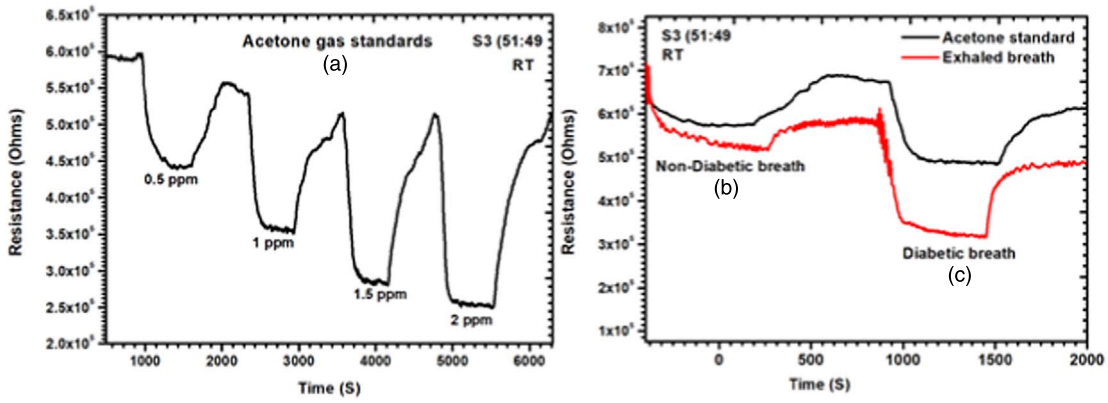

Figure 11. (a) Sensor resistance at room temperature upon exposure to different acetone concentration and non-diabetic (b) and diabetic human breath (c).

Table 2. Gas responses of acetone in the present study and those reported in the literatures.

Material	Fabrication method	Acetone concentration (ppm)	Operating temperature (°C)	Rg/Ra	References
$W0_3$-nanoplates	Topochemical coversation	1000	350	9	[9]
WO_3-nanoplates	Hydrothermal	2000	307	10	[10]
Cr-Wo_3	Flame spray pyrolysis	1	400	2.9	[16]
WO_3-nanotubes	Electrospinning	100	250	40	[24]
Cu-WO_3	Electrospinning	20	300	6.4	[25]
WO_3	Solvothermal	1	100	131	This work

The mechanism of WO_3-based gas sensors has been intensively studied and reported in the literature [3, 9, 10, 44, 45]. Gas sensing mechanism of WO_3 nanoparticles, nanocubes and nanorods sensors is described as follows:

The change in resistance of tungsten oxide sensors is dependent on the adsorbed oxygen species (O^{2-}, O^{-}) on the surface. Upon their exposure to air, O^{2-} gets adsorbed onto the surface which later adsorbs electrons from the conduction band. This decreases the concentration of electrons in conduction band which ultimately decreases the electrical conductance of the material [46]. This mechanism is expressed as follows:

$$O_2(ads) + e^- \rightarrow O^{2-}(ads) \quad (6)$$

$$\boldsymbol{O}^{2-}(ads) + e^- \rightarrow 2O^-(ads) \quad (7)$$

$$\boldsymbol{O}^-(ads) + e^- \rightarrow O^{2-}(ads) \quad (8)$$

In the case where the sensor is exposed to acetone gas, the chemisorbed oxygen species ($O_{2\ (ads)}^-$, $O^{2-}{}_{(ads)}$, $O^-{}_{(ads)}$) react with acetone vapor and releases electrons back to conduction band and as a results, electrical conductance increases. The reaction mechanism is expressed as follows:

$$\mathbf{CH_3COCH_3}(gas) + O^{2-} \rightarrow CH_3C + O + CH_3 + 2e^- \quad (9)$$

$$\mathbf{CH_3C^+O} \rightarrow C^+H_3 + CO \quad (10)$$

$$\mathbf{CO} + \mathbf{O}^{2-} \rightarrow CO_2 + 2e^- \quad (11)$$

In the current study, the enhanced acetone performance of WO_3 indicates that the following parameters played a major role; large pore diameter, high crystallinity, and expedite diffusion channels of WO_3 nanorods. WO_3 nanorods having pore diameter of about 10 nm and high crystallinity were found have excellent acetone-sensing properties than the WO_3 nanoparticles. Since the pore diameter of both nanorods and nanoparticles are mesoporous, gas transport is thought to have occurred through molecular diffusion. This observation is in agreement with the study of Sakai *et al*, which revealed that gas transport in SnO_2 with larger pores occurred mainly through molecular diffusion whereas surface diffusion dominated in micropores. Surface diffusion will have less effect on smaller mesopores [30, 31].

3.8. Breath acetone analysis

Figure 11 shows the resistance curve of sensor S3 at room temperature after injecting acetone standard concentrations of 0.5, 1.0, 1.5, and 2.0 ppm (a), non-diabetic (b) and diabetic breath (c) against standard

acetone. As can be seen, the resistance of the sensor decreased from 5.9 to 4.4 MΩ corresponding to 0.802 response as 0.5 ppm acetone concentration was injected, under 0.39 s. For other concentrations such as 1 ppm, the resistance decreased from 5.3 tap 2.8 MΩ corresponding to 1.4 response, for 1.5 ppm the resistance decreased from 5.0 to 2.8 corresponding to 1.7 response. We further analysed non-diabetic and diabetic breath from a volunteer to assess the performance of the sensor. We have found that with the non-diabetic breath, the resistance decreased from 7.5 to 5.9 MΩ which corresponded to 0.66 response and it was well matched with the response from 0.5 ppm acetone gas standard. This results confirms that the sensor can respond to acetone level in the no-diabetic range (0.8 ppm and below). Furthermore, with the diabetic breath, the sensor's resistance decreased from 5.3 to 3.6 MΩ corresponding to 1.09 response. Interestingly this response ranges with the response observed with 1.0 ppm acetone standard. The results confirms that the sensor can respond well to both non-diabetic and diabetic acetone concentration in human breath.

4. Conclusion

The as-synthesised WO_3 composed of nanoparticles, plate-like structures and nanorods were successfully synthesised by varying solvent content using solvothermal method. The sensor fabricated with 51:49 water: ethanol is found to demonstrate high response and good selectivity to 2 ppm level of acetone when compared with the one fabricated with pure ethanol, 18:92 (ethanol: water) and 92% water. However, the sensor exhibited low response under increased relative humidity at 100 °C. Furthermore, the sensor could response to low concentration of acetone ranging from 0.5 to 4.5 ppm of acetone at 100 °C. More interestingly, the sensor could distinguish the healthy region and diabetic region even under high relative humidity. These characteristics could be attributed to their high pore diameter, crystallite phase which consequently played a major role in the adsorption of oxygen species and enhanced the interactions of acetone and WO_3 on the surface. The gas sensing performance of WO_3 indicates that it has a potential application in low concentration and fast response of acetone detection. These properties are suitable for sensors that can be used for the detection of exhaled acetone from human breath, more specifically in diabetic patients.

Acknowledgments

The authors would like to acknowledge CSIR-DST, project number (HGER85x) for the financial support.

ORCID iDs

Valentine Saasa https://orcid.org/0000-0001-7807-3435
Amos Akande https://orcid.org/0000-0002-3691-9233
Bonex Mwakikunga https://orcid.org/0000-0003-1307-5338

References

[1] Ponzoni A, Comini E, Sberveglieri G, Zhou J, Deng S Z, Xu N S, Ding Y and Wang Z L 2006 Ultrasensitive and highly selective gas sensors using three-dimensional tungsten oxide nanowire networks *Appl. Phys. Lett.* **88** 203101
[2] Akiyama M, Tamaki J, Miura N and Yamazoe N 1991 Tungsten oxide-based semiconductor sensor highly sensitive to NO and NO_2 *Chem. Lett.* **20** 1611–4
[3] Chen D *et al* 2011 Effects of morphologies on acetone-sensing properties of tungsten trioxide nanocrystals *Sensors Actuators B* **153** 373–81
[4] Jia Q, Ji H, Wang D, Bai X, Sun X and Jin Z 2014 Exposed facets induced enhanced acetone selective sensing property of nanostructured tungsten oxide *Journal of Materials Chemistry A.* **2** 13602–11
[5] Li Y, Luo W, Qin N, Dong J, Wei J, Li W, Feng S, Chen J, Xu J and Elzatahry A A 2014 Highly ordered mesoporous tungsten oxides with a large pore size and crystalline framework for H2S sensing *Angew. Chem. Int. Ed.* **53** 9035–40
[6] Zhang C, Li L, Hou L and Chen W 2019 Fabrication of Co_3O_4 nanowires assembled on the surface of hollow carbon spheres for acetone gas sensing *Sensors Actuators B: Chem.* **291** 130–40
[7] Liu Z, Liu B, Xie W, Li H, Zhou R, Li Q and Wang T 2016 Enhanced selective acetone sensing characteristics based on Co-doped WO_3 hierarchical flower-like nanostructures assembled with nanoplates *Sensors Actuators B: Chem.* **235** 614–21
[8] Hou L, Zhang C, Li L, Du C, Li X, Kang X and Chen W 2018 CO gas sensors based on p-type CuO nanotubes and CuO nanocubes: morphology and surface structure effects on the sensing performance *Talanta* **188** 41–9
[9] Shi J, Hu G, Sun Y, Geng M, Wu J, Liu Y, Ge M, Tao J, Cao M and Dai N 2011 WO_3 nanocrystals: synthesis and application in highly sensitive detection of acetone *Sensors Actuators B* **156** 820–4
[10] Liu S, Zhang F, Li H, Chen T and Wang Y 2012 Acetone detection properties of single crystalline tungsten oxide plates synthesized by hydrothermal method using cetyltrimethyl ammonium bromide supermolecular template *Sensors Actuators B* **162** 259–68
[11] Chi X, Liu C, Liu L, Li Y, Wang Z, Bo X, Liu L and Su C 2014 Tungsten trioxide nanotubes with high sensitive and selective properties to acetone *Sensors Actuators B* **194** 33–7

[12] Righettoni M, Tricoli A and Pratsinis S E 2010 Thermally stable, silica-doped ε-WO_3 for sensing of acetone in the human breath *Chem. Mater.* **22** 3152–7
[13] Righettoni M, Tricoli A and Pratsinis S E 2010 Si: WO_3 sensors for highly selective detection of acetone for easy diagnosis of diabetes by breath analysis *Anal. Chem.* **82** 3581–7
[14] Wang L, Kalyanasundaram K, Stanacevic M and Gouma P 2010 Nanosensor device for breath acetone detection *Sensor Letters.* **8** 709–12
[15] Zheng H, Ou J Z, Strano M S, Kaner R B, Mitchell A and Kalantar-zadeh K 2011 Nanostructured tungsten oxide–properties, synthesis, and applications *Adv. Funct. Mater.* **21** 2175–96
[16] Shen J, Zhang L, Ren J, Wang J, Yao H and Li Z 2017 Highly enhanced acetone sensing performance of porous C-doped WO_3 hollow spheres by carbon spheres as templates *Sensors Actuators B: Chem.* **239** 597–607
[17] Shi J, Hu G, Sun Y, Geng M, Wu J, Liu Y, Ge M, Tao J, Cao M and Dai N 2011 WO_3 nanocrystals: synthesis and application in highly sensitive detection of acetone *Sensors Actuators B: Chem.* **156** 820–4
[18] Bai X, Ji H, Gao P, Zhang Y and Sun X 2014 Morphology, phase structure and acetone sensitive properties of copper-doped tungsten oxide sensors *Sensors Actuators B* **193** 100–6
[19] Kirss R U and Meda L 1998 Chemical vapor deposition of tungsten oxide *Appl. Organomet. Chem.* **12** 155–60
[20] Li Y B, Bando Y, Golberg D and Kurashima K 2003 WO_3 nanorods/nanobelts synthesized via physical vapor deposition process *Chem. Phys. Lett.* **367** 214–8
[21] Liu J, Dong X, Liu X, Shi F, Yin S and Sato T 2011 Solvothermal synthesis and characterization of tungsten oxides with controllable morphology and crystal phase *J. Alloys Compd.* **509** 1482–8
[22] Epifani M, Comini E, Díaz R, Genç A, Andreu T, Siciliano P and Morante J R 2016 Acetone sensors based on TiO_2 nanocrystals modified with tungsten oxide species *J. Alloys Compd.* **665** 345–51
[23] Huang J, Xu X, Gu C, Yang M, Yang M and Liu J 2011 Large-scale synthesis of hydrated tungsten oxide 3D architectures by a simple chemical solution route and their gas-sensing properties *J. Mater. Chem.* **21** 13283–9
[24] Konvalina G and Haick H 2013 Sensors for breath testing: from nanomaterials to comprehensive disease detection *Acc. Chem. Res.* **47** 66–76
[25] Saasa V, Malwela T, Beukes M, Mokgotho M, Liu C and Mwakikunga B 2018 Sensing technologies for detection of acetone in human breath for diabetes diagnosis and monitoring *Diagnostics.* **8** 12
[26] Minh T D C, Blake D R and Galassetti P R 2012 The clinical potential of exhaled breath analysis for diabetes mellitus *Diabetes Res. Clin. Pract.* **97** 195–205
[27] Phillips M, Cataneo R N, Saunders C, Hope P, Schmitt P and Wai J 2010 Volatile biomarkers in the breath of women with breast cancer *J. Breath Res.* **4** 026003
[28] Righettoni M, Tricoli A, Gass S, Schmid A, Amann A and Pratsinis S E 2012 Breath acetone monitoring by portable Si: WO_3 gas sensors *Anal. Chim. Acta* **738** 69–75
[29] Dweik R A and Amann A 2008 Exhaled breath analysis: the new frontier in medical testing *J. Breath Res.* **2** 030301
[30] Saasa V, Beukes M, Lemmer Y and Mwakikunga B 2019 Blood ketone bodies and breath acetone analysis and their correlations in type 2 diabetes mellitus *Diagnostics.* **9** 224
[31] Trinh T T, Tu N H, Le H H, Ryu K Y, Le K B, Pillai K and Yi J 2011 Improving the ethanol sensing of ZnO nano-particle thin films—The correlation between the grain size and the sensing mechanism *Sensors Actuators B* **152** 73–81
[32] Pierre G S, Ebihara W T, Speiser R and Pool M J 1962 *TUNGSTEN-OXYGEN SYSTEM, TRANSACTIONS OF THE METALLURGICAL SOCIETY OF AIME.* **224** 259
[33] Sale F R 1979 Heat capacities of the tungsten oxides WO_3, W20O58, W18O49 and WO_2 *Thermochim. Acta* **30** 163–71
[34] Wang Z, Hu M, Wei Y, Liu J and Qin Y 2016 Low-temperature NO_2-sensing properties and morphology-controllable solvothermal synthesis of tungsten oxide nanosheets/nanorods *Appl. Surf. Sci.* **362** 525–31
[35] Zeng X C, Bergman D J, Hui P M and Stroud D 1988 Effective-medium theory for weakly nonlinear composites *Physical Review B.* **38** 10970
[36] Tshabalala Z P, Motaung D E, Mhlongo G H and Ntwaeaborwa O M 2016 Facile synthesis of improved room temperature gas sensing properties of TiO_2 nanostructures: effect of acid treatment *Sensors Actuators B: Chem.* **224** 841–56
[37] Low M 1960 Kinetics of chemisorption of gases on solids *Chem. Rev.* **60** 267–312
[38] Tomer V K, Singh K, Kaur H, Shorie M and Sabherwal P 2017 Rapid acetone detection using indium loaded WO_3/SnO_2 nanohybrid sensor *Sensors Actuators B: Chem.* **253** 703–13
[39] Maswanganye M W, Rammutla K E, Mosuang T E and Mwakikunga B W 2017 The effect of Co and In combinational or individual doping on the structural, optical and selective sensing properties of ZnO nanoparticles *Sensors Actuators B: Chem.* **247** 228–37
[40] Bochenkov V E and Sergeev G B 2010 Sensitivity, selectivity, and stability of gas-sensitive metal-oxide nanostructures *Metal oxide nanostructures and their applications.* **3** 31–52
[41] Rout C S, Hegde M, Govindaraj A and Rao C 2007 Ammonia sensors based on metal oxide nanostructures *Nanotechnology* **18** 205504
[42] Chen Y, Zhu C L and Xiao G 2006 Reduced-temperature ethanol sensing characteristics of flower-like ZnO nanorods synthesized by a sonochemical method *Nanotechnology* **17** 4537
[43] Wang L, Teleki A, Pratsinis S E and Gouma P I 2008 Ferroelectric WO_3 nanoparticles for acetone selective detection *Chem. Mater.* **20** 4794–6
[44] Khadayate R S, Sali J V and Patil P P 2007 Acetone vapor sensing properties of screen printed WO_3 thick films *Talanta* **72** 1077–81
[45] Song C, Li C, Yin Y, Xiao J, Zhang X, Song M and Dong W 2015 Preparation and gas sensing properties of partially broken WO_3 nanotubes *Vacuum* **114** 13–6
[46] Zhang Y, He W, Zhao H and Li P 2013 Template-free to fabricate highly sensitive and selective acetone gas sensor based on WO_3 microspheres *Vacuum* **95** 30–4